Exploring strategies for enhancing magnetoelectric effects in piezoelectric polymer-magnetostrictive nanoparticle systems

Journal of Alloys and Compounds 1047 (2025) 184832

Contents lists available at ScienceDirect

Journal of Alloys and Compounds

journal homepage: www.elsevier.com/locate/jalcom

Exploring strategies for enhancing magnetoelectric effects in piezoelectric polymer-magnetostrictive nanoparticle systems

Gabriele Barrera *, Paolo Allia, Paola Tiberto

INRiM, Advanced Materials Metrology and Life Sciences, Torino, Italy

ARTICLE INFO

Keywords:
Magnetoelectric nanocomposites
Magnetostrictive nanoparticles
Magnetic anisotropy

ABSTRACT

Magnetoelectric 0-3 type nanocomposites for biomedical applications comprised of a piezoelectric polymer and homogeneously dispersed magnetostrictive nanoparticles are investigated with the aim of enhancing the electrical effects elicited by an ac magnetic field. Magnetically blocked magnetite and cobalt ferrite nanoparticles are modelled by means of the rate-equation method, and the magnetoelectric effect is calculated from the elastic and piezoelectric properties of the host polymer. A high value of the nanoparticle magnetostriction constant is shown not to be an essential prerequisite for generating a large electric signal. The magnetoelectric response is improved by adding a magnetic bias field and by varying the amplitude of the ac field, so that the nonlinear region of the magnetostrictive strain can be effectively explored and an optimum working point assuring the best magnetoelectric performance can be defined for each material. The electric response of the nanocomposites is significantly enhanced by collinear instead of randomly directed easy axes of the dispersed nanoparticles; in the collinear case, an analytic expression of the magnetoelectric effect is derived.

1. Introduction

The huge development of advanced materials with multifunctional properties at the nanoscale, such as associations of nanoparticles, nanostructures and nanocomposites, makes it possible to exploit the interplay of diverse effects to achieve a specific aim with unprecedented efficacy. This opportunity plays a pivotal role in activities intended to cure human diseases on novel grounds, like personalized medicine and nanomedicine [1–4]: advanced therapies and cell-culture techniques can now be envisaged, based on the combination of ad hoc properties of nanoscale materials [5–7].

Electroactive media are a promising class of multifunctional biomaterials [8] eligible for a variety of therapeutic applications stemming from controlled electrostimulation of cells [9,10] and including nerve regeneration [11], bone and cardiac tissue engineering [12] and stem-cell fate regulation [13]. In particular, biomaterials based on the piezoelectric effect have attracted much attention in recent years [14] owing to their ability to positively affect the behaviour of cells and tissues [10]. The electrical properties mechanically or magnetically elicited in a piezoelectric biomaterial are credited to play a major role in nerve regeneration, bone healing [15], skin repair [16] and to stimulate proliferation, differentiation and connection of cells, therefore easing self-repair processes in the body [14,17,18].

In *magnetoelectric* materials the electric polarization is mediated by the elastic strain generated by magnetostrictive nanostructures driven by a magnetic field [19–21]. These nanomaterials include 0-0 type magnetoelectric particles comprised of a magnetostrictive core and a piezoelectric shell [21–24], whose role in non-invasive brain cell stimulation has been envisaged [25], demonstrated [26] and elucidated [27]. Core–shell magnetoelectric nanoparticles have been exploited as well in the catalytic degradation of organic compounds [28]. However, the performance of core–shell systems may be affected by the imperfect transmission of the magnetostrictive strain to the piezoelectric shell [27]. In principle, the magneto-piezoelectric transduction which is at the basis of the functional behaviour of these materials can be more easily controlled in two-phase, 0-3 type magnetoelectric nanocomposites comprised of a piezoelectric host (typically, a flexible polymer film) loaded with a dispersion of magnetostrictive nanoparticles. In this way a cheap, non-metallic, flexible membrane with good magnetoelectric properties can be obtained [10,19,29].

Recent applications of magnetoelectric membranes or scaffolds are based on the electric charge magnetically induced at the surface of the material, which activates cell regeneration for bone defect repair [30] and can have antimicrobial effects in cell cultures [31]. Likewise, cell proliferation is enhanced by the presence of positively or negatively charged membrane surfaces [32]. Magnetoelectric membranes drive the dynamic response of cells in the process of osteogenic differentiation [33]. The time-dependent electric polarization of a piezoelectric film can favour the controlled release of drugs [34]. Finally,

* Corresponding author.
E-mail address: g.barrera@inrim.it (G. Barrera).

https://doi.org/10.1016/j.jallcom.2025.184832
Received 25 November 2024; Received in revised form 13 October 2025; Accepted 1 November 2025
Available online 7 November 2025

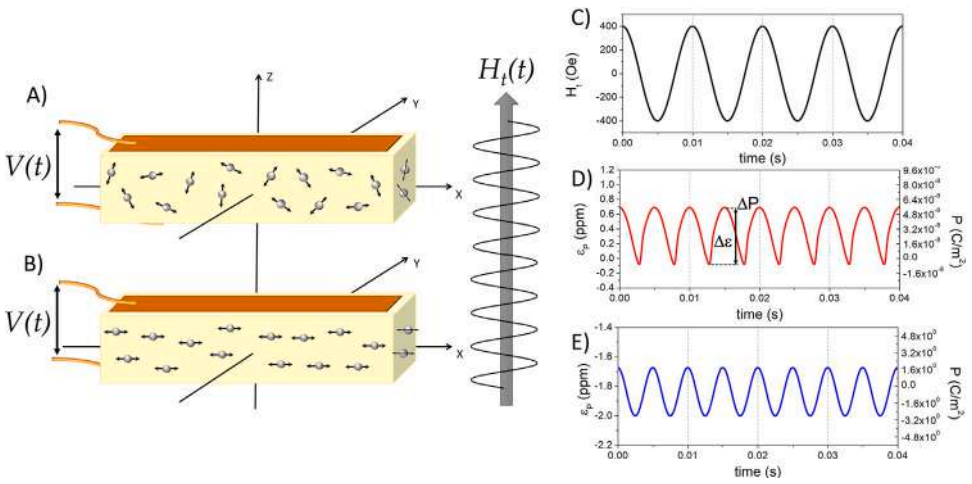

Fig. 1. (*A,B*) configuration of the PVDF film and direction of the total magnetic field for random (*A*) and collinear (*B*) directions of the nanoparticle easy axes; (*C*) applied field waveform; (*D,E*) waveforms of the resulting elastic strain/polarization of the film for random and collinear easy axes, respectively. The peak-to-peak value of elastic strain/polarization of the polymer is defined in panel *D*.

magnetoelectric membranes may find application in transcutaneous stimulation of peripheral nerves and in local treatment of pain [35,36]. Although most applications of magnetoelectric nanocomposites are in biomedicine, a rollable, piezoelectric polymer loaded with magnetic nanoparticles has been demonstrated to act as an energy harvester able to capture the environmental magnetic noise produced by home appliances and to store energy in a commercial capacitor [37,38].

Theoretical models of the behaviour of 0-3 polymer matrix magnetoelectric nanocomposites include approaches based on the solution of the mechano-electrical constitutive equations through either the Green's function method [39,40] or finite element analysis [41]. Another approach is based on the representative volume element method [42,43] and includes a treatment of magneto-rotational effects also; the ensuing calculations are made numerically using the finite-element method. All models bring new elements towards full understanding of the magnetoelectric response, paying however little attention to the details of the magnetic processes underlying the magnetostrictive behaviour of the nanoparticles. In particular, the dependence of magnetization on the applied magnetic field is considered to be either linear or non-hysteretic, which is an oversimplification of a more complex behaviour [27,44].

As a matter of fact, the role of magnetic effects at the nanometer scale on the magnetoelectric behaviour of 0-3 polymer matrix nanocomposites is still to be clarified. In particular, there is no clear understanding of the actual impact of different mechanisms which can be envisaged as main sources of the magnetoelectric effect, which include pure magnetostriction of magnetic nanoparticles and the mechanical reaction of the host polymer to the tendency of particles to rotate under the effect of an applied field [42,43] or the one of small particle aggregates to rearrange under the combined effect of dipolar interaction and applied field [45].

The reason for conducting the present theoretical research is exactly to investigate the magnetoelectric effect in 0-3 polymer matrix nanocomposites which results from pure magnetostriction of nanoparticles, starting from the knowledge of their magnetic properties and behaviour. Such a standpoint will serve to clarify how the performance of these magnetoelectric materials can be effectively enhanced. In this paper, the strategies resulting in an enhancement of the magnetoelectric effect are explored by modelling both the behaviour of the filler under a magnetic field of arbitrary amplitude and the magnetic-to-electric signal conversion mediated by the piezoelectric and elastic properties of the polymer host. The following Sections will investigate the diverse conditions allowing to optimize the magnetoelectric performance in terms of choice of magnetic nanoparticles, configuration of magnetic fields and direction of the particle anisotropy axis. A central role will be shown to be played by the amplitude of the ac magnetic field, allowing to explore the nonlinear region of the magnetostrictive response of dispersed magnetic nanoparticles.

2. General framework

2.1. Materials, properties and design

The magnetoelectric material under study is a film of piezoelectric polymer containing a volume fraction f_V of monodisperse, non-aggregated magnetostrictive nanoparticles, assumed not to appreciably modify the elastic properties of the host material. The physical dimensions of the film are in the centimeter range in the (X, Y) plane, whereas the thickness is of the order of a few hundreds of micrometers as sketched (not to scale) in Fig. 1(A, B). A time-dependent magnetic field $H_t(t)$ is applied perpendicular to the film. As a consequence of the interplay between the magnetostrictive properties of nanoparticles and the piezoelectric response of the host polymer, a time-dependent electric polarization is generated within the film, so that an ac voltage (of frequency twice the one of the magnetic field) appears between the planar surfaces and can be measured (see Fig. 1(A, B), where two alternative configurations of the easy axes of magnetic anisotropy of the embedded nanoparticles, indicated by the arrows, are shown).

The magnetic nanoparticles are assumed to be spheroidal and magnetically blocked at room temperature. Generally speaking, blocked (i.e., non superparamagnetic) nanoparticles display a magnetic hysteresis [44]; at zero magnetic field the magnetization of each nanoparticle lies along the local easy axis of magnetic anisotropy [46]. All nanoparticles are tightly embedded in the host polymer, so that their physical translation or rotation are forbidden and the magnetic properties can only evolve through Néel's relaxation [47], a feature that allows to use a rate-equation formalism for magnetic double-level systems (DWS) [48] to predict the time-dependent magnetic and magnetostrictive properties in equilibrium and off-equilibrium systems of nanoparticles. A summary of principles and validity of the rate-equation method can be found in the Supporting Information.

The magnetoelectric properties of these nanocomposites are of course to be optimized with an eye of regard for practical applications, including the biomedical ones; such an aim can be achieved in different, if somewhat intermingled, ways: *a* by selecting the magnetostrictive nanoparticles that perform best in the operating conditions typical of each considered application, and *b* by looking for the most effective distribution of their easy axes within the nanocomposite. Most of the

Table 1
Size, volume fraction and magnetic/magnetostrictive parameters of magnetite and cobalt ferrite nanoparticles used in this work.

	Fe_3O_4	$CoFe_2O_4$
Size (nm)	16	7
f_V	0.1	0.1
M_s (emu/cm^3)	350	300
K_{eff} (erg/cm^3)	3×10^5	3×10^6
λ_s	40×10^{-6}	-110×10^{-6}

Table 2
Stiffness matrix elements C_{ij} in PVDF (10^9 N/m^2); piezoelectric matrix elements d_{ij} (10^{-12} C/N); values of the G constant defined in Eq. (13) (C/m^2).

C_{11}	6.43
C_{12}	4.25
d_{31}	18
d_{32}	5
d_{33}	−26
G	-8.03×10^{-2}

research works of the recent literature on magnetoelectric biomaterials [23,49] deal with nanoparticles of cobalt ferrite ($CoFe_2O_4$), mainly because this material is characterized by a high isotropic magnetostriction constant $\lambda_s \approx -110 \times 10^{-6}$; in some cases, nanoparticles made of magnetite (Fe_3O_4, $\lambda_s \approx 40 \times 10^{-6}$) have been investigated also [23,24].

Both magnetic nanoparticles will be dealt with in this paper; their size, volume fraction and properties are given in Table 1. It should be reminded that the effective anisotropy constant K_{eff} associated to a nanoparticle can take into account, in a simplified way, the weak dipolar interaction among distant magnetic dipoles [50]. It is easy to check that magnetite and cobalt ferrite nanoparticles of the selected diameters and characterized by the values of K_{eff} reported in Table 1 are indeed magnetically blocked at room temperature.

The piezoelectric host is assumed to be a uniaxially oriented film of polyvinylidene fluoride (PVDF), a commercial piezoelectric polymer having very good piezo-, pyro-, and ferroelectric activity with prospective applications in various sectors [51]. The β phase of PVDF guarantees an optimal piezoelectric response by effect of a mechanical stress applied from outside [52], with applications including wearable tactile sensors and force/pressure sensors [52,53]. The piezoelectric properties of PVDF allow make this polymer attractive in applications such as tissue engineering, surgery techniques, drug delivery, implants as well as in energy harvesting [54]. The values of the mechanical and piezoelectric of the PVDF film of interest for us are given in Table 2; the film is assumed to have a rectangular shape and a uniform thickness of 200 nm. The properties of two magnetoelectric nanocomposites containing a volume fraction $f_V = 0.10$ of either magnetite or cobalt ferrite nanoparticles embedded in the β phase of PVDF will be studied; they will be referred to as ME_m and ME_c, respectively.

The typical magnetoelectric behaviour of these nanocomposite materials is sketched in Fig. 1($C-E$). An ac magnetic field of the type $H_{ac}(t) = H_v \cos \omega t$ (in this example $H_v = 400$ Oe, $f = \omega/2\pi = 100$ Hz, panel C) generates in the film a periodic elastic strain along the Z direction and consequently an ac polarization $\boldsymbol{P}$ directed along Z whose modulus is proportional to the strain (Fig. 1(D, E) refers to the different configurations of the easy axes shown in panels (A, B), respectively; see Sections 3 and 4). The exact shape of the induced strain/polarization signal depends on many factors, including the features of the applied magnetic field (amplitude and frequency) and the ones of the magnetostrictive nanoparticles, such as the shape of the hysteresis loop and the distribution of the easy axis directions in the film; the frequency of the electric signal is twice that of the magnetic field. A central role is played by the peak-to-peak value of the strain generated by the nanoparticles in the nanomaterial, $\Delta\epsilon_P$. which is proportional to the peak-to-peak amplitude of the polarization ΔP, both defined in Fig. 1D.

A parameter measuring the quality of the magnetoelectric effect is the average magnetoelectric (ME) coefficient which can be defined as:

$$\alpha_{ME} = \frac{\Delta E}{\Delta H} = \frac{1}{2\epsilon_0 \epsilon_r} \frac{\Delta P}{H_v} \tag{1}$$

where ΔE is the peak-to-peak value of the electric field inside the material and ϵ_r is the relative permittivity of the medium around the piezoelectric film. The second equality holds because in this case $\Delta E = \Delta P/\epsilon_0\epsilon_r$ (see Section 3.1) and $\Delta H = 2H_v$.

The design of the magnetoelectric nanocomposite examined in this paper implies a perfect transduction of the mechanical effect from magnetic nanoparticles to the polymer, as resulting from ideal, flawless interfaces between magnetostrictive and piezoelectric phases. As a matter of fact, the problem of the degradation of the α_{ME} coefficient in biphasic magnetoelectric materials by effect of a non-ideal mechanical contact at the interfaces [55] has been debated since the development of sintered ME composites [56,57]. The factors affecting mechanical contact between the functional phases are mainly of crystallographic and elastic nature (including lattice mismatch, dissimilar elastic compliances [57], mechanical defects such as pores at the interface between the two phases [55]). The influence of the interface has been specifically analysed in the case of magnetostrictive–piezoelectric bilayers, where the friction between the contacting films plays an important role [58]. In this case, owing to the simpler geometry, a theoretical study of the quality of the mechanical transduction has been done, and a single interface coupling parameter has been defined [58]. In particular, the ME coefficient was predicted to be linearly reduced from the ideal value with decreasing the coupling parameter, which is basically a measure of the differential deformation between magnetostrictive and piezoelectric layers.

Presumably even in nanocomposites where the polymeric piezoelectric phase incorporates the magnetostrictive nanoparticles, the condition of ideal interfaces is hardly fulfilled in practice, so that the amplitudes of the effects analysed in this paper should be viewed as upper limit values.

2.2. Condition for maximum magnetostrictive strain

The ME behaviour of 0-3 nanocomposites is strongly dependent on the amplitude of the magnetostrictive strain generated in magnetic nanoparticles. It is possible to evaluate the maximum strain produced in a magnetostrictive nanoparticle by a magnetic field able to rotate the magnetization vector away from the easy axis. As discussed elsewhere [27], the magnetostrictive deformation ϵ of a blocked nanoparticle along the field's direction is assumed to depend on a single-valued magnetostriction constant λ_s and on the squared cosine of the angle between $\boldsymbol{M}$ and the direction $\boldsymbol{u}_t$ of the applied field $\boldsymbol{H}_t = H_t \boldsymbol{u}_t$, according to the expression:

$$\epsilon \equiv (\Delta l/l) = \frac{3}{2}\lambda_s \left[\cos^2 \widehat{\boldsymbol{M}\boldsymbol{u}_t} - \frac{1}{3}\right] \tag{2}$$

Therefore ϵ takes its maximum value ($\epsilon_\infty = \lambda_s$), when $\boldsymbol{M}$ is parallel to $\boldsymbol{u}_t$, i.e., at magnetic saturation (in principle, for $H_t \to \pm\infty$). The magnetostrictive strain at $H_t = 0$ (ϵ_0) depends on the angle between the easy axis (where the magnetization lies) and $\boldsymbol{u}_t$; the lowest possible value corresponds to the condition $\boldsymbol{M} \perp \boldsymbol{u}_t$, in which case $\epsilon_{0\perp} = -\frac{1}{2}\lambda_s$. As a consequence, the maximum possible strain of a magnetostrictive nanoparticle along the direction of the applied field is $\Delta\epsilon = |\epsilon_\infty - \epsilon_{0\perp}| = \frac{3}{2}|\lambda_s|$.

As a matter of fact, such an ideal result can only be attained by applying to the nanoparticle a harmonic field of very large amplitude ensuring that magnetic saturation is reached; in other words, the ac field $H_{ac}(t)$ should explore the whole major hysteresis loop of the nanoparticle. However, meeting such a condition (which implies producing an ac magnetic field of several thousands of Oe) can be

both technically difficult and energy consuming. One could therefore investigate if it is possible to attain, or at least closely approach, the maximum value of the peak-to-peak strain of a set of nanoparticles (i.e., $\frac{3}{2}|\lambda_s|$) without making use of a very large ac field. In fact, an effective strategy is to apply a collinear dc bias field H_b so that the total field along Z becomes:

$$H_t(t) = H_b + H_{ac}(t) = H_b + H_v \cos \omega t \tag{3}$$

A dc bias field of magnitude up to several thousands of Oe can be easily produced at low costs and can be tuned to produce a total field H_t that explores different regions of the $M(H_t)$ curve of the nanoparticles. Such a device has been already discussed and implemented in actual measurements on magnetoelectric films [26,59–61].

The effect of the interplay between bias and ac field will be shown in the following Sections, where two configurations respectively corresponding to random and collinear directions of the easy axes of the nanoparticles embedded in the PVDF film will be separately treated.

3. Random easy axes of nanoparticles

When the nanoparticles are dissolved in the fluid precursor of the polymer without applying an external magnetic field, their easy axes are expected to point along all directions of space in the polymerized material, as depicted in Fig. 1*A*. An order-of-magnitude calculation reveals that a weak dipolar interaction among magnetic nanoparticles of the considered sizes is not able to keep their easy axes aligned during the process of polymerization.

The total magnetic field $H_t(t)$ defined in Eq. (3) is assumed to be perpendicular to the film. In present-day biomedical applications of piezoelectric and magnetoelectric nanomaterials, the frequency of the driving force (either mechanical or magnetic) producing the biologically relevant polarization of the material is between a few Hz to about 10 kHz [10]. The magnetostrictive response of both magnetite and cobalt ferrite nanoparticles has been preliminarily tested by us in the interval $1 \le f \le 1 \times 10^4$ Hz, and found not to be a strong function of the ac field frequency, as shown in the Supporting information (Figures S1 and S2). Therefore, the ensuing calculations will be all done using an ac field of frequency $f = 100$ Hz, an intermediate value deemed to be representative of the magnetostrictive response in the entire range of frequencies used in applications. It is assumed that the amplitudes of both the bias field and the ac field can be independently varied. The bias field H_b is taken as positive and can vary from zero to several thousands of Oe, a range easily attained by standard laboratory techniques.

An ac magnetoelastic strain $\epsilon_P(t)$ of frequency $2f = 200$ Hz is generated in the polymer along the field direction (the Z axis), so that an ac polarization $\boldsymbol{P}$ parallel to $\boldsymbol{H}_t$ and of amplitude proportional to ϵ_P appears in the piezoelectric film; a detailed calculation of the magnetoelectric effect is given in the following Section.

3.1. Magnetoelectric effect

Magnetite or cobalt ferrite nanoparticles of diameters $D = 16$ and $D = 7$ nm respectively are assumed to be uniformly dispersed in the β phase of a PVDF film with easy axes pointing in all directions; the nanoparticles are both physically constrained by the polymer and magnetically blocked, so that for zero magnetic field the magnetization vector is everywhere aligned to the particle's easy axis.

The piezoelectric film lies in the (X, Y) plane and the total magnetic field $\boldsymbol{H}_t = H_t \boldsymbol{u}_Z$ is applied along the Z axis, as shown in Fig. 2. Each nanoparticle is characterized by three local Cartesian axes (1,2,3) defined as follows:

(a) axis 3 is directed along the field;

(b) axis 1 is in the plane defined by the particle's easy axis and axis 3;

(c) axis 2 is perpendicular to both axis 1 and axis 3.

As a consequence, axes (1,2) randomly point along all directions in the (X, Y) plane, whereas axis 3 is always parallel to the applied field. The easy-axis direction of a particle is defined by two angles (θ, ϕ) with respect to the (X, Y, Z) axes: θ $(0 \le \theta \le \pi)$ is the colatitude measured from the Z axis, ϕ $(0 \le \phi \le 2\pi)$ is the azimuth measured from the X axis.

Under a magnetic field, the magnetization vector of each nanoparticle rotates away from the easy axis towards the field by an angle $\delta = \delta(\theta, H_t)$; the rotation is always in the (1,3) plane. For a given value of H_t and for a given θ, the angle δ is obtained by solving the DWS model.

The general expression of the magnetostrictive strain ϵ_u of each nanoparticle along any direction $\boldsymbol{u}$ is:

$$\epsilon_u \equiv (\Delta l/l)_u = \frac{3}{2}\lambda_s \left[\cos^2 \widehat{\boldsymbol{M}\boldsymbol{u}} - \frac{1}{3}\right] \tag{4}$$

which applies when the particles are magnetically blocked, i.e., not in the superparamagnetic state [27]. In particular, when the strain $\epsilon_u \equiv \epsilon_Z$ is measured along the field direction ($\boldsymbol{u} \equiv \boldsymbol{u}_t \equiv \boldsymbol{u}_Z$), Eq. (4) becomes equal to Eq. (2), which can be easily rewritten as:

$$\epsilon_Z(\theta, H_t) = \frac{3}{2}\lambda_s \left[\cos^2\big(\theta - \delta(\theta, H_t)\big) - \frac{1}{3}\right] \tag{5}$$

(see Fig. 2). Applying the same rule it is possible to find the strain along the other two local Cartesian axes; the strain along the X-axis is:

$$\epsilon_X(\theta, \phi, H_t) = \frac{3}{2}\lambda_s \left[\cos^2\gamma - \frac{1}{3}\right] = \frac{3}{2}\lambda_s \left[\sin^2\big(\theta - \delta(\theta, H_t)\big)\cos^2\phi - \frac{1}{3}\right] \tag{6}$$

The second equality is obtained expressing $\cos\gamma$ in terms of angles (θ, ϕ) [27]. By analogy:

$$\epsilon_Y(\theta, \phi, H_t) = \frac{3}{2}\lambda_s \left[\sin^2\big(\theta - \delta(\theta, H_t)\big)\sin^2\phi - \frac{1}{3}\right] \tag{7}$$

Averaging ϵ_X, ϵ_Y over all values of angle ϕ and taking into account that $\overline{\cos^2\phi} = \overline{\sin^2\phi} = 1/2$, it can be immediately observed that $\overline{\epsilon}_X(\theta, H_t) = \overline{\epsilon}_Y(\theta, H_t) = -\frac{1}{2}\epsilon_Z(\theta, H_t)$, as expected.

The average of $\epsilon_Z(\theta, H_t)$ over the colatitude θ is:

$$\langle \epsilon_Z(H_t) \rangle = \frac{1}{2}\int_0^\pi \epsilon_Z(\theta, H_t)\sin\theta\, d\theta \tag{8}$$

This quantity is the average strain along the Z axis of the magnetite nanoparticles generated by the applied magnetic field $\boldsymbol{H}_t = H_t \boldsymbol{u}_Z$. In order to simplify the notation, let us call $\langle \epsilon_Z(H_t) \rangle = \epsilon$. Assuming that the strain produced by a fraction f_V of nanoparticles dispersed in the PVDF film is effectively and evenly transmitted to the piezoelectric material [27], the deformation ϵ_P of the polymer along the direction of $\boldsymbol{H}_t$, is expected to be $\epsilon_P = f_V \epsilon$. It should be explicitly recalled that the oscillation frequency of ϵ_P is twice the one of $H_t \equiv H_b + H_v \cos(\omega t)$.

The off-diagonal elements of the (3×3) strain tensor ϵ_{ij} $(i, j = 1, 2, 3)$ in the PVDF film are equal to zero because the magnetic field is assumed not to be a source of a significant shear strain neither in the nanoparticles nor in the polymer [27], whereas the diagonal elements are $\epsilon_{11}, \epsilon_{22} = -f_V\epsilon/2, \epsilon_{33} = f_V\epsilon$; using the Voigt contracted notation, the (6×1) strain vector $\boldsymbol{\epsilon_P}$ of the PVDF film is therefore:

$$\boldsymbol{\epsilon_P} = \begin{pmatrix} -\frac{1}{2}f_V\epsilon \\ -\frac{1}{2}f_V\epsilon \\ f_V\epsilon \\ 0 \\ 0 \\ 0 \end{pmatrix} \tag{9}$$

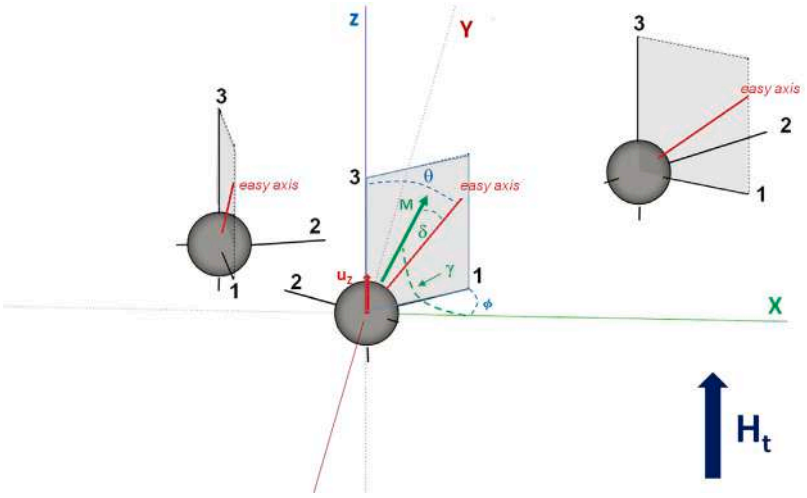

Fig. 2. Sketch of three magnetic nanoparticles having different easy-axis directions in the polymer. The (1,2,3) axes define the reference frame attached to each nanoparticle; the local easy axis is always in the (1,3) plane. The (X, Y, Z) axes are the principle axes of the polymer film. The quantities used in the calculations of Section 3.1 are defined for the nanoparticle in the foreground.

The (6×1) stress vector $\boldsymbol{\sigma_P} = [\boldsymbol{C}] \cdot \boldsymbol{\epsilon_P}$ is obtained using the (6×6) stiffness/elastic matrix $\boldsymbol{[C]}$ appropriate to PVDF, whose structure is [62]:

$$[\boldsymbol{C}] = \begin{pmatrix} C_{11} & C_{12} & C_{12} & 0 & 0 & 0 \\ C_{12} & C_{11} & C_{12} & 0 & 0 & 0 \\ C_{12} & C_{12} & C_{11} & 0 & 0 & 0 \\ 0 & 0 & 0 & C_{33} & 0 & 0 \\ 0 & 0 & 0 & 0 & C_{33} & 0 \\ 0 & 0 & 0 & 0 & 0 & C_{33} \end{pmatrix} \tag{10}$$

Therefore:

$$\boldsymbol{\sigma_P} = [\boldsymbol{C}] \cdot \boldsymbol{\epsilon_P} = \begin{pmatrix} -\frac{1}{2}(C_{11} - C_{12}) f_V \epsilon \\ -\frac{1}{2}(C_{11} - C_{12}) f_V \epsilon \\ (C_{11} - C_{12}) f_V \epsilon \\ 0 \\ 0 \\ 0 \end{pmatrix} \tag{11}$$

Finally, the (3×1) polarization vector in the polymer is obtained by applying to the vector $\boldsymbol{\sigma_P}$ the 3rd rank direct piezoelectric matrix $[\boldsymbol{d}]$ of dimensions (3×6), whose structure in the present case is:

$$[\boldsymbol{d}] = \begin{pmatrix} 0 & 0 & 0 & 0 & d_{15} & 0 \\ 0 & 0 & 0 & d_{15} & 0 & 0 \\ d_{31} & d_{32} & d_{33} & 0 & 0 & 0 \end{pmatrix} \tag{12}$$

As it turns out,

$$\boldsymbol{P} = [\boldsymbol{d}] \cdot \boldsymbol{\sigma_P} = \begin{pmatrix} 0 \\ 0 \\ \left[d_{33} - \frac{1}{2}(d_{31} + d_{32})\right](C_{11} - C_{12}) f_V \epsilon \end{pmatrix} \equiv \begin{pmatrix} 0 \\ 0 \\ G f_V \epsilon \end{pmatrix} \tag{13}$$

Therefore, a uniform polarization directed along the Z axis is generated in the PVDF film. The numerical values of the C_{ij} have been calculated using the elastic constants for the β phase of a PVDF film [63]; the d_{ij} matrix elements have been taken from Ref. [63]; the constant G is calculated using its definition (Eq. (13)) and are listed in Table 2.

The magnetization M_P of the nanocomposite film as well as the peak-to-peak values of the elastic strain $\Delta\epsilon_P$ and of the associated polarization ΔP generated within the polymer film (graphically defined in panel *d* of Fig. 1) are related in a simple way to the magnetization M and magnetostrictive strain $\Delta\epsilon$ of the embedded magnetic nanoparticles:

$$\begin{cases} M_P = f_V \ M \\ \Delta\epsilon_P = f_V \, \Delta\epsilon \\ \Delta P = f_V \, |G| \, \Delta\epsilon_P \end{cases} \tag{14}$$

where $f_V = 0.10$ and $|G|$ is the piezoelectric parameter calculated for the β phase of PVDF (see Table 2).

Therefore, the polarization vector is proportional to ϵ and oscillates in phase with the strain of the set of nanoparticles. Considering the PVDF film similar to a parallel-plate capacitor immersed in a medium of relative permittivity ϵ_r, the oscillating electric field inside the film has peak-to-peak value $\Delta E = \Delta P / \epsilon_0 \epsilon_r$. Using $\epsilon_r \approx 1$, the magnetoelectric coefficient α_{ME} of the nanocomposite polymer turns out to be:

$$\alpha_{ME} = \frac{\Delta E}{\Delta H_v} = 9.07 \times 10^9 \, f_V \, \frac{\Delta\epsilon}{\Delta H_v} \tag{15}$$

where ΔH_v is expressed in Oersted.

3.2. Symmetric curves of magnetization and polarization

Let us start by studying the ME effect of the ac magnetic field in the absence of bias field ($H_b = 0$). When the amplitude of the driving field is very small, the ME behaviour can be approximately described in terms of the linear response theory (corresponding to the limit $H_v \to 0$) [64–67]. However, nonlinearities inherent to the magnetic and magnetostrictive behaviour of the embedded nanoparticles [27,44] develop when the ME material is submitted to an ac magnetic field of arbitrary amplitude. In the considered frequency region (≈ 100 Hz) the ac field amplitude H_v can in principle be increased up to values of the order of 1×10^4 Oe; the maximum value is basically suggested by technical limitations and cost reasons. Exiting the linear regime makes the problem more difficult to deal with but paves the way to a significant improvement of the ME response.

The hysteresis loops of the magnetization M_P and of the strain ϵ_P of the nanocomposite film along the field direction (obtained using Eq. (2)) are calculated by solving the rate equations for the random distribution of easy axes. The results for M_P are shown in Fig. 3(A, B) (orange lines), whereas the ϵ_P curves are reported in Fig. 3(C–F) (black lines). The upward/downward curvature of ϵ_P curves is ascribed to the different sign of the magnetostriction constant in the two materials. The strain/field curves turn out to be fully reversible above the so-called *closure field* of the magnetization, i.e., when the nanoparticle magnetization begins to change through fully reversible processes only [46].

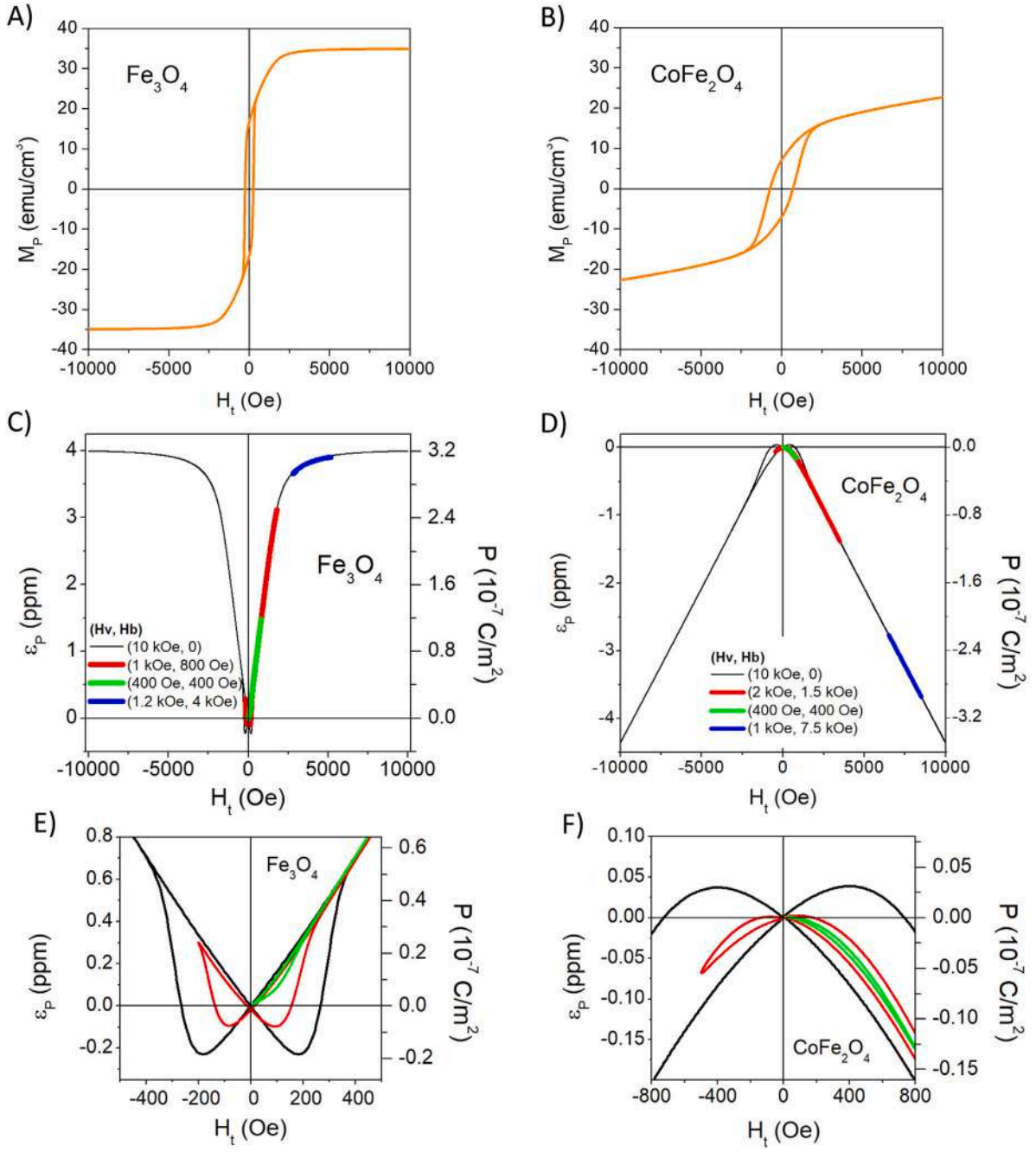

Fig. 3. (*A,B*) magnetic hysteresis loops of the nanocomposites loaded with magnetite and cobalt ferrite nanoparticles for $H_b = 0$ and $H_v = 10$ kOe; (*C,D*) examples of the elastic strain/polarization curves as functions of the total applied field for some pairs of bias and ac field amplitudes; (*E,F*) enlargements of panels (*C,D*) showing the hysteresis at low fields.

Hysteresis of $\epsilon_P(H_t)$ appears in the low-field region, as shown in panels (E, F) (black lines).

According to the discussion of Section 2.2, the maximum (in absolute value) $\Delta\epsilon_{P\,Max}$ of the magnetostrictive strain in the nanocomposite is expected to occur for $H_t \to \infty$ and is equal to the product $f_V\,|\lambda_s|$ (i.e., 4×10^{-6} in ME_m and 11×10^{-6} in ME_c). It can be observed that in the first case (panels A, C) the field $H_{tM} \equiv H_{vM}$ is enough to bring both the magnetization and the elastic strain almost to saturation, so that the maximum of the $\epsilon_P(H_t)$ curves for $H_t = H_{tM}$ is very close to 4×10^{-6}. This is no longer true in the film containing cobalt ferrite nanoparticles (panels B, D), mostly owing to the much larger value of the magnetic anisotropy K_{eff}: the value of ϵ_P measured at H_{tM} is far from the ideal maximum $f_V\,|\lambda_s| = 11 \times 10^{-6}$.

The magnetostrictive strain and the polarization of the nanocomposite are hysteretic functions of the applied field because both effects stem from the hysteretic behaviour of magnetically blocked nanoparticles. The two branches of the symmetric loop of P cross in $H_t = 0$, where $\epsilon_P = 0$ (when $H_t = 0$, i.e., at the magnetic remanence of the magnetization, the mean value of the squared cosine in Eq. (2) is equal to 1/3). In the ME_m nanocomposite, the minimum of the $\epsilon_P(H_t)$ curve (which is observed to occur when H_t is close to the coercive field of the magnetization loop) is slightly negative (panel E), so that the maximum amplitude of the strain variation $\Delta\epsilon_{P\,Max}$ is slightly larger than $f_V\,|\lambda_s|$. Although a similar behaviour, with reversed signs, is observed in ME_c, in this material the largest observed value of $\Delta\epsilon_P$ turns out to be considerably less than the product $f_V\,|\lambda_s|$.

3.3. Effects of bias and ac field. Optimum working conditions.

As observed in Section 2.2, the region of total fields investigated by setting $H_b = 0$ and $H_v = H_{vM}$ can be explored in a different (and energetically more convenient) way by exploiting the bias field. The effect of independently varying the bias field amplitude as well as the ac field amplitude is shown in Fig. 3($C-F$) for both ME$_m$ and ME$_c$. Even in this case, the results were obtained following the calculation scheme outlined in Section 3.1 and numerically solving the rate equations of the DWS model.

Changing the bias field, different intervals of the total field are explored, centred at different values of H_t; as a consequence, the $\epsilon_P(H_t)$ curves are now asymmetric with respect to the vertical axis (the only symmetric curve being the one at $H_b = 0$). Three examples of results obtained by using different values of both H_b and H_v are given in Fig. 3(B, C) for each material (short lines in colour). The explored segments of the $\epsilon_P(H_t)$ curves exactly overlap to the master curve obtained when $H_b = 0$ (black line), at least for fields larger than the closure field of the $M_P(H_t)$ curve. This effect is explained considering that in this region the strain is a reversible function of the total magnetic field $H_t = H_b + H_{ac}(t)$. On the other hand, the curves no longer overlap in the low-field region where the hysteresis of ϵ_P appears, as shown in panels (E, F).

The shape of these asymmetric curves is related to the one of the loops of M_P, which are shown in Figure S3 of the Supporting Information. Generally speaking, with increasing H_b the hysteresis loops of both M_P and ϵ_P become increasingly asymmetric and narrower; above the closure field the strain ϵ_P becomes a fully reversible function of the total field. During each cycle of the driving field, ϵ_P (and P) follow back and forth the paths in colour of Fig. 3($C - F$), as it becomes apparent when the behaviour of both quantities is reported in the time domain (as in Figure S4 of the Supporting Information).

To our knowledge, experimental results on 0-3 type magnetoelectric polymers have been taken so far by using small ac field amplitudes (up to 25 Oe) [45,65–71]. The curves of Fig. 3 show that the magnetoelectric effect may be substantially enhanced by increasing the ac field amplitude and concurrently using a bias field of proper amplitude. In principle, there are no technical limitations to build coils able to generate ac magnetic fields up to several hundreds of Oe at low frequencies (≈ 100 Hz); in such a frequency region, an ac field of large amplitude does not produce harmful or discomforting effects in the human body [72]. Our results suggest that new regions of the strain/field curve should be experimentally explored in order to improve the magnetoelectric response.

The behaviour of the peak-to-peak values $\Delta\epsilon_P$ and ΔP as functions of the bias field H_b is shown in Fig. 4(A, B) for the two polymer films and for selected values of the amplitude of $H_{ac}(t)$.

In the ME$_m$ nanocomposite (panel A), the $\Delta P(H_b)$ curves calculated for $H_v \lessapprox 2 \times 10^3$ Oe display a substantial increase up to a single maximum (ΔP^*) when H_b is increased from zero, and a slow decrease towards zero for larger H_b values. When the ac field amplitude is increased, ΔP^* increases and its position H_b^* shifts towards right, as also shown in Figure S5 of the Supporting Information. The shape of the $\Delta_P(H_b)$ curves significantly changes with changing H_v, reflecting the complex effect of varying both the width and the centre of the explored region of the hysteresis loop.

When $H_v \gtrapprox 2 \times 10^3$ Oe, the magnetoelectric effect becomes increasingly less dependent on the bias field; in particular, the $\Delta P(H_b)$ curve reduces to a horizontal straight line when $H_v = H_{vM}$. In this case the peak-to-peak values of both strain and polarization in the polymer are already saturated for $H_b = 0$ (i.e., $\Delta\epsilon_P \equiv \Delta\epsilon_{P\,Max}$ and $\Delta P \equiv \Delta P_{Max} = f_V\,|G|\,\lambda_s$), as shown by looking at the black curve in panel C of Fig. 3; therefore, adding a bias field does not have any further effect on the magnetoelectric response. The saturation value $\Delta\epsilon_{P\,Max}$ is equal to about 4.2×10^{-6} for a volume fraction of nanoparticles $f_V = 0.10$. This value results from the difference between the maximum positive strain of magnetite nanoparticles (corresponding to $\lambda_s = 40 \times 10^{-6}$) and the negative strain around the coercive field, which turns out to be $\approx -2 \times 10^{-6}$ for $H_v = H_{vM}$.

On the other hand, in ME$_c$ a field as large as H_{vM} is still not enough to saturate the magnetoelectric signal (Fig. 4B), as already observed in Fig. 3D, so that all the $\Delta P(H_b)$ curves show a single maximum at intermediate H_b values. Even in this case the shape of the curves changes with increasing H_v, the magnitude of ΔP^* increases and its position H_b^* is displaced towards right, as shown in Figure S5 of the Supporting Information.

By comparing the results for the two materials, the following conclusions can be drawn:

(a) in both piezoelectric nanocomposites, a suitable choice of H_b enhances the ME effect with respect to the case $H_b = 0$ (at least when the amplitude of $H_{ac}(t)$ is not enough to bring ΔP to saturation);

(b) the positions H_b^* of the maxima of the ME effect ΔP^* are in quite different regions; as a rule, much lower bias fields are needed to maximize the effect in ME$_m$;

(c) departing from the linear regime ensures that the induced polarization ΔP may take values comparable to the maximum theoretical value ΔP_{Max};

(d) in the nonlinear regime, when H_v is below $\approx 1{\times}10^3$ Oe, the peak-to-peak value of ΔP at $H_b = 0$ turns out to be systematically higher in the ME$_m$ nanocomposite than in ME$_c$, in spite of the larger value of the magnetostrictive constant in cobalt ferrite; for instance, for $H_v = 400$ Oe and $H_b = 0$ the magnetoelectric effect is 20 times higher in ME$_m$; the same feature is preserved when a bias field is applied (when $H_v = 400$ Oe ΔP^* is still four times higher in ME$_m$);

Therefore, for the same volume fraction of embedded nanoparticles and for an ac field of amplitude not exceeding a few hundreds of Oe, dissolving magnetite nanoparticles in the PVDF film is preferable to choosing cobalt ferrite nanoparticles. Such a counterintuitive conclusion is not unexpected [27], the physical reason being that cobalt ferrite nanoparticles have not only a high magnetostriction but also a high magnetic anisotropy (the two properties are of course correlated [46]). As a consequence, in cobalt ferrite nanoparticles the applied field is not able to appreciably rotate the magnetization away from the local easy axis, resulting in a very small strain along the Z direction; for the same reason much larger fields are needed to trigger the rotation.

The positive effect of the dc bias field on the response of a magnetoelectric material was already experimentally observed [26,64,73,74]; the present model allows us to give a quantitative description of the effect. It should be stressed that for each choice of H_v an optimum value (or an optimum region of values) of the bias field exists, corresponding to the maximum of the ME effect, so that for each magnetoelectric nanocomposite an *optimum working point* can be defined; such a condition is basically determined by the magnetic properties of the dispersed magnetic nanoparticles. Knowing such an optimum working point allows the user to tune the amplitudes of both applied fields in order to get the best magnetoelectric response at the minimum possible energy cost for a given type of dispersed nanoparticles. In this way a significant ME effect can be generated by substituting a single dynamic field of large amplitude (difficult to produce and rather energy-consuming) with the effect of the interplay of a small dynamic field and a static field of large amplitude, both easier to produce and operate.

A pictorial representation of the behaviour of the magnetoelectrical effect in the (H_b, H_v) plane and of the optimum working point is shown in Fig. 4(C, D). There, the surfaces represent the values of $\Delta P(H_b, H_v)$ calculated when the amplitudes of the two fields are continuously varied within ranges typical of normal operating conditions.

The difference between the effects of the two types of magnetostrictive nanoparticles is apparent by comparing panels C and D: the lower magnetic anisotropy of magnetite nanoparticles results in a much faster approach to the saturation value ΔP_{Max} as the amplitude of the ac field is increased, as indicated by the steep rise of the effect in Fig. 4C. At saturation, a large plateau is observed, indicating that

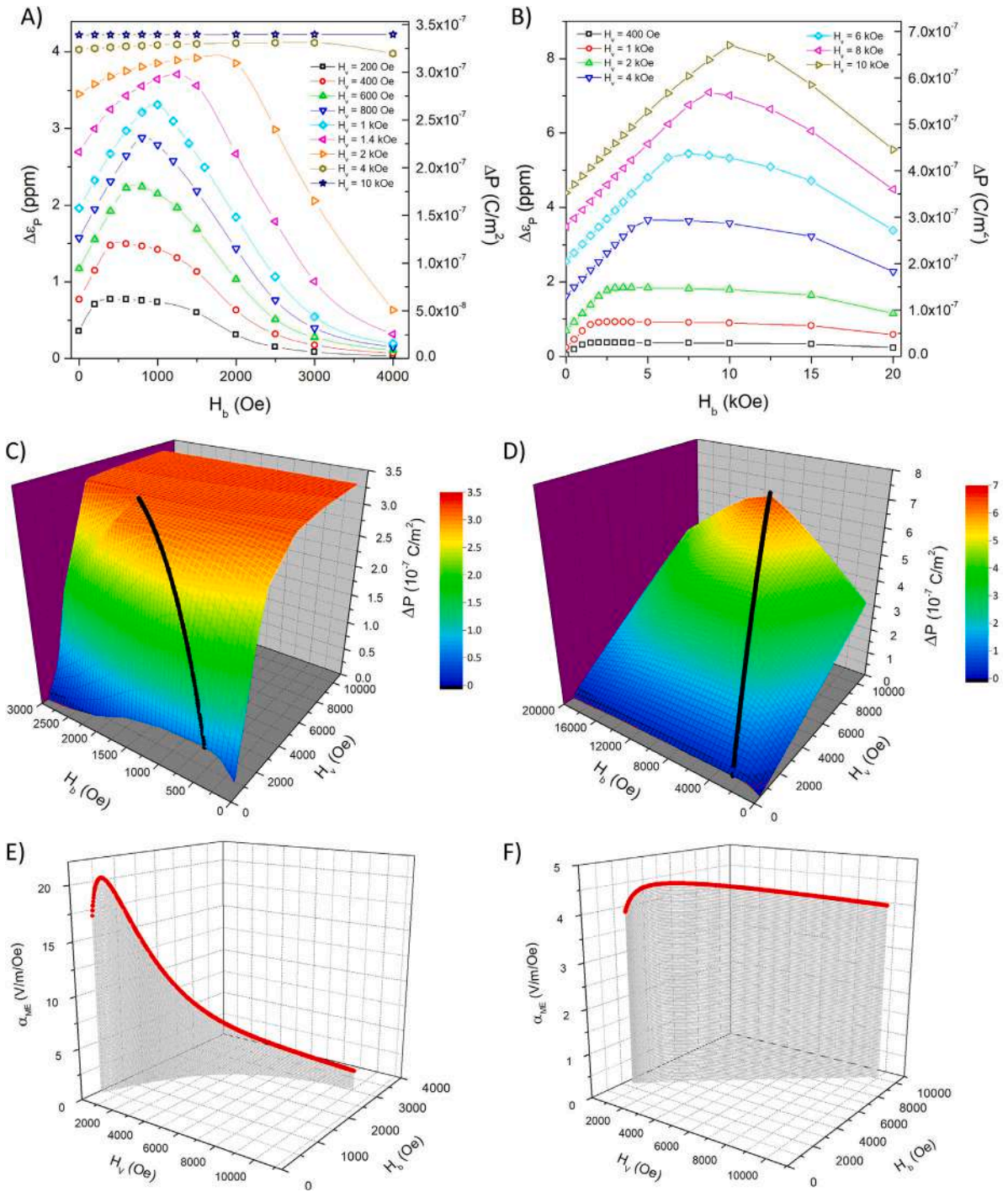

Fig. 4. Random easy axes. (*A,B*) Peak-to-peak values $\Delta\epsilon_P$, ΔP of elastic strain and polarization of nanocomposites containing magnetite (*A*) and cobalt ferrite (*B*) nanoparticles as functions of the bias field amplitude H_b and for different values of the ac field amplitude H_v; (*C,D*) surfaces showing the behaviour of the magnetoelectric effect ΔP in the (H_b, H_v) plane for the two materials; the black line is the locus of the optimum working point for each pair of (H_b, H_v) values; (*E,F*) behaviour of the magnetoelectric coefficient $\alpha_{ME}(H_b, H_v)$ at the optimum working point for the two materials.

the magnetoelectric effect is no longer influenced by the amplitude of either the bias field or the ac field. On the other hand, the large magnetic anisotropy of cobalt ferrite nanoparticles results in a smoother surface associated to a gentle rise of the effect with increasing both H_b and H_v (Fig. 4*D*).

The black dots superimposed to each surface indicate the locus of the maxima of the magnetoelectric effect for each choice of the ac field amplitude, i.e., the optimum working point. In the case of ME_m (Fig. 4*C*) the line is interrupted as soon as the plateau of ΔP is reached, i.e., for $\Delta P \rightarrow \Delta P_{Max}$. In this case the bias field is unable to further modify the magnetoelectric response of the polymer, and can be set to zero. As expected, the ME_m nanocomposite gives a better ME response, at least in the range of magnetic-field amplitudes corresponding to actual measurements and applications; in particular, the quantity ΔP_{Max} becomes higher in ME_c than in ME_m only for ac field amplitudes $H_v \gtrapprox 4$ kOe, a value much higher than the ones used in typical measurements (see Figure S5 of the Supporting Information).

Table 3
Experimental values of the magnetoelectric coefficient of some 0-3 polymer matrix ME nanocomposites.

ME nanocomposites	α_{ME} ($Vm^{-1}Oe^{-1}$)	Ref.
$CoFe_2O_4$/PVDF	0.2	[77]
$CoFe_2O_4$/P(VDF-TrFE)	4	[78]
$CoFe_2O_4$/P(VDF-TrFE)	0.2 – 1	[65]
$CoFe_2O_4$/PVDF	0.65 – 0.75	[79]
$ZnFe_2O_4$/PVDF	0.06	[80]
$Zn_{0.2}Co_{0.8}Fe_2O_4$/PVDF	1.4	[69]
$CoFe_2O_4$/P(VDF-TrFE)	1 – 4.5	[66]
$Zn_{0.2}Co_{0.8}Fe_2O_4$/P(VDF-TrFE)	1.5	[81]
$NiFe_2O_4$/P(VDF-TrFE)	1.1 – 1.5	[68]
Fe_3O_4/P(VDF-TrFE)	4.5 – 6.7	[70]
Fe_3O_4/P(VDF-TrFE)	0.9	[67]
$YFeO_3$/PVDF	0.32 – 0.52	[82]
$LaYFe_2O_6$/P(VDF-HFP)	0.29	[83]
$LiFe_5O_8$/PVDF-HFP	2.0	[84]

The maximum of the induced polarization ΔP^* obtained at the optimum working point for each choice of H_v (black dots in Fig. 4(C, D)), results in an ac voltage $\Delta V = \Delta P^* t_F/(\epsilon_0\epsilon_r)$ across the nanocomposite (whose thickness is assumed to be $t_F = 200\,\mu m$; see Section 3.1). Taking $\epsilon_r \approx 1$, the resulting voltage turns out to be in the 1.4 V - 7.8 V range in ME_m and between 0.6 V and 15.4 V in ME_c for the investigated range of bias and ac field amplitudes. In the low-field region these values are comparable to the voltage generated in a PVDF film of comparable thickness submitted to a mechanical stress [75,76].

The behaviour of the average magnetoelectric coefficient α_{ME} at the optimum working point is shown in Fig. 4(E, F) for the two nanocomposites. The magnetoelectric coefficient turns out to be significantly higher in ME_m than in ME_c, as expected. These results are in line with the ones of similar composite systems reported in the recent literature [8,21]. The curves display a single absolute maximum corresponding to the optimal choice of both H_b and H_v. In ME_m the $\alpha_{ME}(H_b, H_v)$ curve is peaked around the maximum at $H_v = 386$ Oe, $H_b = 550$ Oe where it takes a value as high as $\approx$ 20 V/m/Oe and quickly drops towards zero; in ME_c the curve is much less structured, its maximum ($\approx$ 4.5 V/m/Oe) being at $H_v = 2110$ Oe , $H_b = 3836$ Oe. In the latter case the choice of the best pair of (H_v, H_b) values is not so critical as in ME_m.

As a matter of fact, for both nanocomposites the maximum α_{ME} in the nonlinear regime turns out to be not dramatically larger than the value calculated in the linear regime ($H_v \to 0$) under a suitable bias field (see Figure S6 of the Supporting Information). Therefore, in regard to the ME material's ability to efficiently respond to the driving field, entering the nonlinear regime does not result in a striking improvement with respect to the linear case; however, it should be stressed that the important parameter in applications is the magnitude of the electrical polarization induced in the material, which is greatly enhanced when operating in nonlinear conditions (at the cost of making use of a significantly larger driving field).

Typical experimental values of the magnetoelectric coefficient α_{ME} in 0-3 polymer matrix ME nanocomposites are reported in Table 3.

The results were mainly obtained on nanocomposites containing cobalt-ferrite nanoparticles; both the intrinsic properties of magnetic particles (size, composition, concentration, aggregation) and the experimental conditions (ac field amplitude and frequency, bias field amplitude) were considerably different from case to case. This circumstance contributes to the high dispersion of values, which can be noticed even in materials with the same nominal composition, as in the cases discussed below:

- the magnetite nanoparticles dispersed in P(VDF-TrFE) (see Table 3) strongly differ in size and consequently in their magnetic behaviour: the nanoparticles of Ref. [67] have a size of 20 nm and are in the dc superparamagnetic regime, whilst the ones of Ref. [70] have a size of 50 nm and are in the magnetically blocked state. The different magnetic regimes bring about markedly different responses to the ac field [27], whose amplitude is in addition twice larger in Ref. [70] (10 Oe) than in Ref. [67] (5 Oe). This circumstance results in different magnetostrictive strains and consequently in different ME coefficients;
- on the other hand, the cobalt-ferrite nanoparticles dispersed in PVDF (see Table 3) have strongly different diameters (about 10 nm in Ref. [79] and in the range 20–100 nm in Ref. [77]); this fact entails a completely different effect of the bias field on the ME coefficient: the higher ME coefficient of Ref. [79] is reported to correspond to the absolute maximum of the $\alpha_{ME}(H_b)$ curve at $\approx$1 kOe, whereas in Ref. [77] the absolute maximum of the $\alpha_{ME}(H_b)$ curve is not yet attained in the explored bias field range (up to 5 kOe);
- in P(VDF-TrFE) containing cobalt-ferrite nanoparticles (Refs. [65, 78] in Table 3) the same fillers were used; in this case the different measured values can be mainly ascribed to the different amount of dispersed particles (20% and 72%, respectively).

Although the magnetoelectric effect is enhanced by operating at the optimum working point, this is not enough to reach the highest theoretical value of the magnetoelectric effect, ΔP_{th}. Using and recalling the discussion of Section 2.2, it is immediate to show that $\Delta P_{th} = \frac{3}{2}|\lambda_s| f_V |G| = 4.82 \times 10^{-7}$ C/m^2 in the ME_m nanocomposite and $\Delta P_{th} = 13.25 \times 10^{-7}$ C/m^2 in ME_c.

Inspection of Fig. 4($A-D$) shows that even at the optimum working point the highest ΔP values are far below ΔP_{th} in both nanocomposites. For instance, the highest magnetoelectric effect generated in the ME_m nanocomposite turns out to be only about two thirds of ΔP_{th}. This is explained by realizing that the maximum magnetoelectric effect generated in the film by a set of nanoparticles with random easy axes is intrinsically limited to a value close to $|\lambda_s| f_V |G|$.

As the limiting effect is inherently related to the random distribution of the nanoparticles' easy axes, a further enhancement of the magnetoelectric response is only possible by achieving a different easy-axis configuration in the polymer.

4. Collinear easy axes

As previously determined, the peak-to-peak strain of a single magnetic nanoparticle is maximized when the angle between the direction of the magnetization at zero applied field (coincident with the easy axis of the nanoparticle) and the magnetic field $\boldsymbol{H}_t$ is equal to $\pi/2$ (see Eq. (4)). If the magnetic nanoparticles dispersed in the PVDF film have random easy axes, such a condition is in general not fulfilled. Therefore, an efficient method to get a good performance of a magnetoelectric nanocomposite based on PVDF is to control the directions of the easy nanoparticle axes during the process of fabrication of the material; in particular, the easy axes should be collinear and parallel to the film, as sketched in Fig. 1B. In principle, such a configuration can be obtained by applying a strong static magnetic field $\boldsymbol{H}_a$ during the process of formation of the material. In this Section only the ME_m nanocomposite will be studied, owing to the many advantages of magnetite nanoparticles with respect to cobalt ferrite nanoparticles, particularly at low values of the ac field amplitude.

As a matter of fact, a perfect alignment of the easy axes can only be achieved by applying a very large magnetic field; however, fields of the order of some thousands of Oe should be enough to give rise to substantially collinear magnetite nanoparticles with $D = 16$ nm; here, the ideal condition of perfect alignment will be discussed. The nanoparticles are supposed to be evenly separated in the polymer matrix; in fact, with the considered values of size, magnetization and volume fraction of the particles, and taking into account the high viscosity of the fluid precursor of the polymer, the formation of nanoparticle chains with aligned easy axes by effect of long-range particle displacements can be ruled out [85,86].

When the nanoparticle axes are collinear and perpendicular to $\boldsymbol{H}_t$, the magnetization and the magnetoelectric effect of the nanocomposite have simple analytic solutions, as discussed in next Section.

4.1. Magnetization and magnetoelectric effect

All easy axes are now assumed to be aligned with the X axis, i.e., they are perpendicular to $\boldsymbol{H}_t$. Such a configuration, corresponding to $\theta = \pi/2$, gives the maximum magnetostrictive effect of magnetically blocked nanoparticles. On the contrary, in the parallel configuration ($\theta = 0$) the magnetization of a blocked particle always lies on the easy axis, independent of the value of the applied field, and no strain variation is measured along the Z direction. Both $M(H_t)$ and the magnetostrictive strain ϵ of the nanoparticles are now represented by analytical expressions.

As known [44], when $\theta = \pi/2, \phi = 0$ the populations of the two energy wells of the DWS are always equal to each other and the magnetization of nanoparticles coherently rotates towards the Z axis by an angle $\delta(H_t)$ according to the expressions [46]:

$$\begin{cases} \sin\delta = -1 & (H_t \le -\widetilde{H_t}) \\ \sin\delta = \dfrac{M_s H_t}{2K_{eff}} = \dfrac{H_t}{\widetilde{H_t}} & (|H_t| \le \widetilde{H_t}) \\ \sin\delta = 1 & (H_t \ge \widetilde{H_t}) \end{cases} \tag{16}$$

where $\widetilde{H_t} = 2K_{eff}/M_s$. The magnetization along the field direction is equal to $M_s \sin\delta$, so that:

$$\begin{cases} M(H_t) = -M_s & (H_t \le -\widetilde{H_t}) \\ M(H_t) = \dfrac{M_s^2 H_t}{2K_{eff}} = M_s \dfrac{H_t}{\widetilde{H_t}} & (|H_t| \le \widetilde{H_t}) \\ M(H_t) = M_s & (H_t \ge \widetilde{H_t}) \end{cases} \tag{17}$$

Therefore, the magnetization is a linear, anhysteretic function of the applied field with constant slope between the limits $\pm\widetilde{H_t}$; for larger positive/negative fields M takes the saturation value $M = \pm M_s$, respectively (see Fig. 5*A*). Using the values of Table 1, $\widetilde{H_t} \approx 1710$ Oe for magnetite. The magnetization of the polymer film is $M_P = f_V\, M$ and is shown in Fig. 5*A*, where the $M_P(H_t)$ curve (blue line) is compared with the one obtained in the case of random easy axes (thin orange line).

Using Eq. (5) with $\theta = \pi/2$, one has:

$$\begin{cases} \epsilon_Z(H_t) = \dfrac{3}{2}\lambda_s\left[\sin^2\delta - \dfrac{1}{3}\right] = \dfrac{3}{2}\lambda_s\left[\left(\dfrac{H_t}{\widetilde{H_t}}\right)^2 - \dfrac{1}{3}\right] & (|H_t| \le \widetilde{H_t}) \\ \epsilon_Z(H_t) = \lambda_s & (|H_t| \ge \widetilde{H_t}) \end{cases} \tag{18}$$

The parabolic behaviour of $\epsilon_P(H_t) = f_V\, \epsilon_Z(H_t)$ is shown in Fig. 5*B*. Similarly one gets:

$$\begin{aligned} \epsilon_X &= \frac{1}{2}\lambda_s - \epsilon_Z \\ \epsilon_Y &= -\frac{1}{2}\lambda_s \end{aligned} \tag{19}$$

so that $\epsilon_X + \epsilon_Y + \epsilon_Z = 0$, as expected. Calling $\epsilon_z = \epsilon$ and following the same steps as in Section 3.1, one gets an identical formal expression for the peak-to-peak polarization value $\Delta P = |G| f_V \Delta\epsilon$; however, in the present case $\Delta\epsilon$ can be expressed in an analytical form as a function of the bias field H_b for any amplitude of the ac field H_v. Two different sets of expressions apply to different regions of the ac field amplitude:

I. When $H_v \le \widetilde{H_t}/2$ (≈ 855 Oe for magnetite nanoparticles):

(*a*) $H_b \le H_v$:

$$\Delta\epsilon = \frac{3}{2}\lambda_s\left(\frac{H_b + H_v}{\widetilde{H_t}}\right)^2 \tag{20}$$

(*b*) $H_v \le H_b \le \widetilde{H_t} - H_v$:

$$\Delta\epsilon = 6\lambda_s \frac{H_v H_b}{\widetilde{H_t}^2} \tag{21}$$

(*c*) $\widetilde{H_t} - H_v \le H_b \le \widetilde{H_t} + H_v$:

$$\Delta\epsilon = \frac{3}{2}\lambda_s\left[1 - \left(\frac{H_b - H_v}{\widetilde{H_t}}\right)^2\right] \tag{22}$$

(*d*) $H_b \ge \widetilde{H_t} + H_v$:

$$\Delta\epsilon = 0. \tag{23}$$

It can be easily verified that the strain of the ME$_m$ nanocomposite $\Delta\epsilon_P = f_V\, \Delta\epsilon$ is a continuous function of H_b everywhere, although its derivative is discontinuous. The cusp-like behaviour of $\Delta P(H_b) = |G| f_V \Delta\epsilon(H_b)$ is shown in Fig. 5*C*. The value corresponding to the cusp ΔP^* is attained for $H_b^* = \widetilde{H_t} - H_v$ and has value:

$$\Delta P^* = 6\lambda_s\, |G|\, f_V\, \frac{H_v}{\widetilde{H_t}}\left(1 - \frac{H_v}{\widetilde{H_t}}\right). \tag{24}$$

For a given dispersion of magnetic particles, the above expression only depends on H_v. It is therefore possible to find the amplitude of the ac field which maximizes ΔP^*. The form of Eq. (24) suggests that the absolute maximum of ΔP^* is attained when $H_v/\widetilde{H_t} = \frac{1}{2}$, i.e., $H_v = \widetilde{H_t}/2$, which is the upper limit of the region of H_v values investigated so far. In this case, the polarization of the nanocomposite reaches the value $\Delta P_{Max} = \frac{3}{2} f_V\, |G|\, \lambda_s$ (light blue curve in Fig. 5*C*) .

The ac field amplitude H_v can of course be freely increased above the value $\widetilde{H_t}/2$. In this case, the quantity $\left(\widetilde{H_t} - H_v\right)$ becomes smaller than H_v, so that the analytical expressions for $\Delta\epsilon$ (Eq. (20) to (23)) should be rearranged:

II. When $H_v \ge \widetilde{H_t}/2$

a) $H_b \le \widetilde{H_t} - H_v$:

$$\Delta\epsilon = \frac{3}{2}\lambda_s\left(\frac{H_b + H_v}{\widetilde{H_t}}\right)^2 \tag{25}$$

b) $\widetilde{H_t} - H_v \le H_b \le H_v$:

$$\Delta\epsilon = \frac{3}{2}\lambda_s \tag{26}$$

c) $H_v \le H_b \le \widetilde{H_t} + H_v$:

$$\Delta\epsilon = \frac{3}{2}\lambda_s\left[1 - \left(\frac{H_b - H_v}{\widetilde{H_t}}\right)^2\right] \tag{27}$$

d) $H_b \ge \widetilde{H_t} + H_v$:

$$\Delta\epsilon = 0 \tag{28}$$

Even in this case $\Delta P = f_V\, |G|\, \Delta\epsilon$ is a continuous function of H_b with discontinuous derivative. The cusp is substituted by a large plateau at $\Delta P^* \equiv \Delta P_{Max} = \frac{3}{2} f_V\, |G|\, \lambda_s$, as shown in Fig. 5*C*.

It should be noted that while in the case of randomly directed easy axes the maximum peak-to-peak value of the polarization of the nanocomposite is basically equal to $f_V\, |G|\, \lambda_s$ (see Fig. 3), for collinear easy axes this quantity is enhanced by a factor 1.5, pointing to a definitely better magnetoelectric performance of the piezoelectric polymer. Using collinear easy axes gives the further advantage that full saturation of magnetization and polarization can be attained for a rather small value of the total field.

In the collinear case, an analytic expression can be obtained for the magnetoelectric coefficient α_{ME} too. Taking into account Eqs. (24) and (26), the magnetoelectric coefficient takes the form:

$$\begin{cases} \alpha_{ME} = \dfrac{3\lambda_s |G| f_V}{\epsilon_0 \epsilon_r}\dfrac{1}{\widetilde{H_t}}\left(1 - \dfrac{H_v}{\widetilde{H_t}}\right) & (H_v \le \widetilde{H_t}/2) \\ \alpha_{ME} = \dfrac{3\lambda_s |G| f_V}{4\epsilon_0 \epsilon_r}\dfrac{1}{H_v} & (H_v \ge \widetilde{H_t}/2) \end{cases} \tag{29}$$

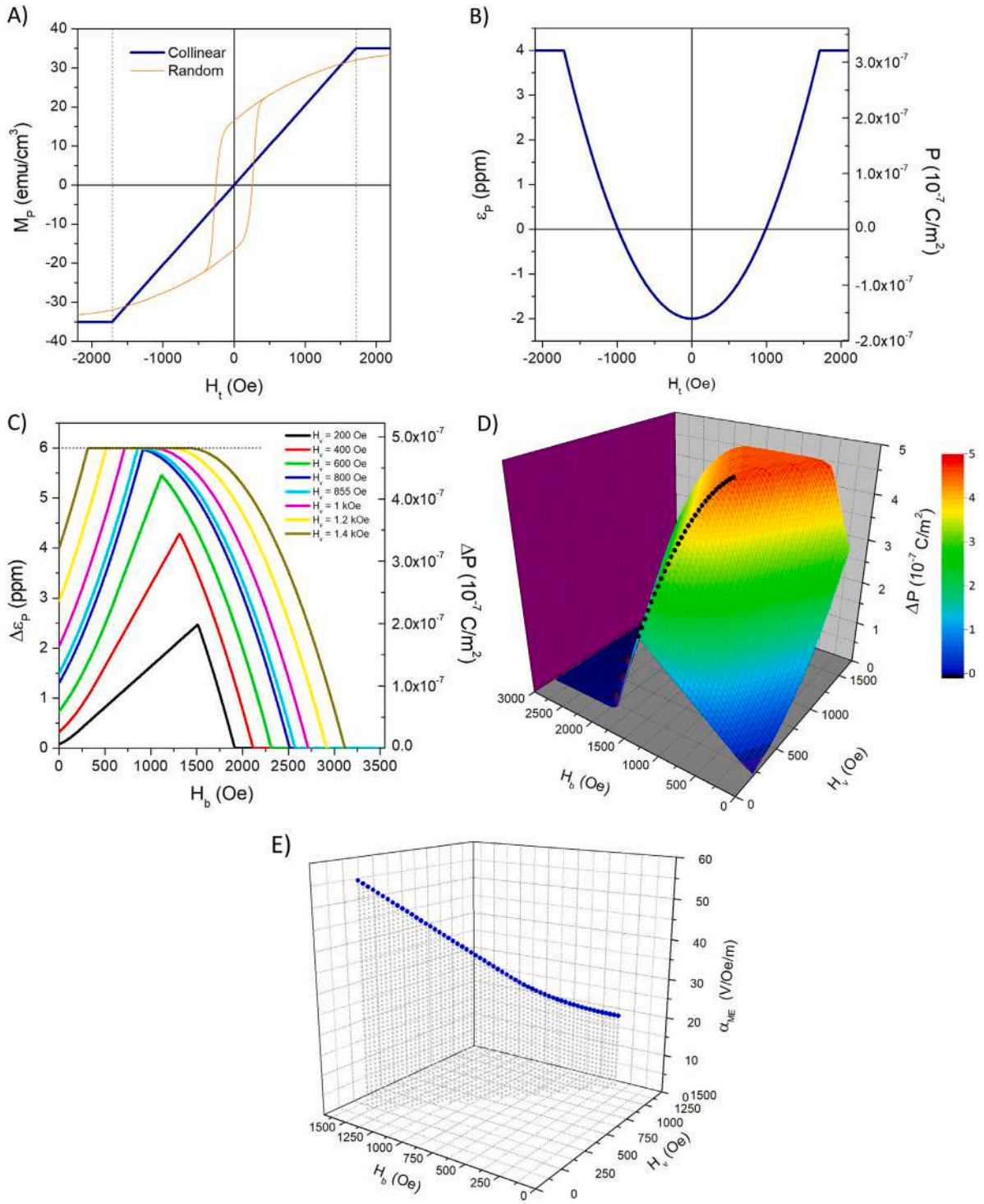

Fig. 5. Collinear easy axes. (*A*) Behaviour of the magnetization with the applied field for the nanocomposite containing magnetite nanoparticles (blue line; the thin orange line is the $M(H_t)$ curve for random easy axes); (*B*) elastic strain/polarization curve as a function of the applied field; (*C*) peak-to-peak values $\Delta\epsilon_P$, ΔP of elastic strain and polarization as functions of the bias field amplitude H_b, for different values of the ac field amplitude H_v; (*D*) surface showing the behaviour of the magnetoelectric effect ΔP in the (H_b, H_v) plane; the black line is the locus of the optimum working point for each pair of (H_b, H_v) values; (*E*) behaviour of the magnetoelectric coefficient $\alpha_{ME}(H_b, H_v)$ at the optimum working point.

Therefore α_{ME} is a continuous function of H_v, monotonically decreasing towards zero from the value:

$$\alpha_{ME,Max} = \frac{3\lambda_s |G| f_V}{\epsilon_0 \epsilon_r} \frac{1}{\widetilde{H_t}} \approx 63.6 \text{ V/m/Oe}$$

corresponding to the limit $H_v \to 0$. In this case, the amplitudes of the bias field and the ac field corresponding to the optimum working point are linearly related by the condition $H_b^* = \widetilde{H_t} - H_v$. The behaviour of α_{ME} is shown in Fig. 5*E*.

4.2. Interplay of bias and ac fields

The whole strain/polarization curve of Fig. 5*B* can be explored by exploiting the interplay between a bias field and the ac field, with the

advantage that analytical expressions exist. The peak-to-peak variation of the magnetostrictive strain of the magnetite nanoparticles ($\Delta\epsilon$), is given in terms of both H_b and H_v by Eqs. (20)–(23) and (25)–(28). $\Delta\epsilon$ is everywhere a continuous function of H_b, although its derivative is discontinuous in places. The resulting behaviour of ΔP as a function of H_b for the ME_m nanocomposite is shown in Fig. 5*C* for different values of H_v. The overall behaviour of ΔP as a function of H_b can be summarized as follows:

- for $H_v \leq \widetilde{H_t}/2 = 855$ Oe, the $\Delta P(H_b)$ curves obtained from Eqs. (20)–(23) display a rise of the magnetoelectric effect up to a cusp-like maximum whose value increases with increasing H_v, whilst its position on the H_b axis moves towards left; beyond the cusp the magnetoelectric effect decreases and goes to zero;

- when $H_v = 855$ Oe (light blue line in Fig. 5*C*), the ΔP value at the cusp reaches the absolute maximum ΔP_{Max} corresponding to $\Delta\epsilon_{P\,Max} = 6 \times 10^{-6}$ (this is the maximum possible strain variation in magnetite nanoparticles);

- for higher values of H_v the cusp transforms into a plateau, whose width increases with increasing H_v and where the magnetoelectric effect is maximized; before the plateau ΔP still increases from the initial value; beyond the plateau ΔP decreases to zero.

It should be remarked that in the present case the cusp of the $\Delta P(H_b)$ curves is gradually displaced towards left with increasing H_v (Fig. 5*C*), whereas the opposite behaviour was found in the case of a random distribution of easy axes (Fig. 4(*A*, *B*)).

The overall behaviour of ΔP in the (H_b, H_v) plane is shown by the colour map of Fig. 5*D*, where the optimum working point is indicated by the dotted black line. Once the plateau of the magnetoelectric effect is attained, both the bias and the ac field are ineffective in further changing the magnetoelectric response of the material, so that one is free to choose the most convenient (e.g., the less energy-consuming) values of the applied fields. It should be taken into account that the plateau of ΔP can be attained using rather low values of both H_b and H_v, indicating that magnetite nanoparticles with collinear axes are particularly suitable to elicit at low costs a large magnetoelectric effect from the host piezoelectric polymer.

In the collinear case, the voltage generated across the ME_m nanocomposite film is between 4.5 and 10.9 V for the considered range of bias and ac field values (to be compared with the interval 1.4 V–7.8 V for randomly distributed easy axes). The magnetoelectric coefficient α_{ME} is a monotonically decreasing function of the sole ac field amplitude H_v, as shown by Eq. (29). The behaviour of α_{ME} in the (H_b, H_v) plane is shown in Fig. 5*E*.

5. Conclusion

We have developed a theoretical framework tailored to 0-3 nanocomposites containing a fraction of magnetically blocked nanoparticles dispersed in piezoelectric PVDF, with the aim of predicting the magnetoelectric response elicited when the material is operating off the linear region, i.e., for arbitrarily large values of the ac magnetic field which drives the effect.

The main results of this study are:

- in the nonlinear regime, the ME behaviour of both nanocomposites is strongly enhanced with respect to the linear case;
- departing from the linear regime, the electrical polarization induced in the ME material can become comparable to the maximum value predicted by theory; even in the nonlinear regime such a result is best achieved by exploiting the interplay of the ac and bias fields;
- an optimum working point where the magnitude of the induced polarization and the magnetoelectric coefficient are maximized is determined in both nanocomposites for an appropriate choice of *both* bias-field and ac-field amplitudes;
- the magnetic nanoparticles eliciting a large magnetoelectric signal are not necessarily the ones having the highest value of the magnetostriction, because the ME response is determined by a complex interplay between the intrinsic magnetic properties of nanoparticles (K_{eff}, λ_s) and the amplitude of the applied magnetic field(s);
- the degree of order of the easy-axis directions of nanoparticles plays a significant role; when the easy axes are aligned, the magnetoelectric effect of the nanocomposites is further enhanced with respect to the case of randomly distributed easy axes.

Although the present theoretical approach only depicts the properties of an idealized, flawless structure, it may help clarify the features of the behaviour of 0-3 type magnetoelectric nanocomposites with the dual aim of explaining the outcomes of new experiments and showing how to enhance the magnetoelectric effect in view of practical applications. To our knowledge, no account of the degradation of the ME coefficient by effect of a less-than-ideal quality of the nanoparticle-polymer interface has been proposed so far. As a matter of fact, the actual degree of structural/mechanical matching at the interface is still an open issue, and an assessment of the quality of the interface should be an important task of future investigations.

CRediT authorship contribution statement

Gabriele Barrera: Writing – review & editing, Writing – original draft, Validation, Investigation, Conceptualization. **Paolo Allia:** Writing – review & editing, Writing – original draft, Investigation, Formal analysis, Conceptualization. **Paola Tiberto:** Writing – review & editing, Validation, Investigation.

Declaration of competing interest

The authors declare that they have no known competing financial interests or personal relationships that could have appeared to influence the work reported in this paper.

Appendix A. Supplementary data

Supplementary material related to this article can be found online at https://doi.org/10.1016/j.jallcom.2025.184832.

References

[1] Xina Yi Wong, Amadeo Sena-Torralba, Ruslan Alvarez-Diduk, Kasturi Muthoosamy, Arben Merkoçi, ACS Nano 14 (2020) 2585–2627.
[2] Benjamin Nottelet, Sytze Buwalda, Cornelusa F. van Nostrum, Xiaofei Zhao, Chao Deng, Zhiyuan Zhong, Ernest Cheah, Darren Svirskis, Chloe van Trayford, Sabine Rijt, J. Phys.: Mater. 7 (2023)) 012502.
[3] Ganeshlenin Kandasamy, Dipak Maity, Mater. Sci. Eng.: C 127 (2021)) 112199.
[4] Ashkan Bigham, Atefeh Zarepour, Arezoo Khosravi, Siavash Iravani, Ali Zarrabi, Mater. Today Sustain. (2024)) 100865.
[5] Deepa Suhag, Swati Kaushik, Taxaka Vinod Bala, Handbook of Biomaterials for Medical Applications, 1, Springer Nature, 2024).
[6] Annan Chen, Wanying Wang, Yunhu Mao, Shiting Chen, Guo Liu, Jin Su, Pei Feng, Yusheng Shi, Chunze Yan, Adv. Mater. 36 (2024) 2307686.
[7] Ritesh Kumar, Ipsita Pattanayak, Pragyana Aparajita Dash, Smita Mohanty, J. Mater. Sci. 58 (2023)) 3460–3484.
[8] Pedro Martins, Ricardo Brito-Pereira, Sylvie Ribeiro, Lanceros-Mendez Senentxu, Clarisse Ribeiro, Nano Energy (2024)) 109569.
[9] Kausik Kapat, Quazia TH Shubhra, Miao Zhou, Sander Leeuwenburgh, Adv. Funct. Mater. 30 (2020) 1909045.
[10] Zhirong Liu, Xingyi Wan, Zhonga Lin Wang, Linlin Li, Adv. Mater. 33 (2021)) 2007429.
[11] Soumitra Das, Thimukondaa Jegadeesan Jeyapriya, Bikramjit Basu, ACS Biomater. Sci. Eng. 10 (2024)) 1620–1645.
[12] Maria Kitsara, Andreu Blanquer, Gonzalo Murillo, Vincent Humblot, Sara Dea Bragança Vieira, Carme Nogués, Elena Ibáñez, Jaume Esteve, Leonardo Barrios, Nanoscale 11 (2019)) 8906–8917.

[13] Maria Guillot-Ferriols, Carlosa M. Costa, Danielaa M. Correia, Joséa Carlos Rodríguez-Hernández, Penelopea M. Tsimbouri, Senentxu Lanceros-Méndez, Matthewa J. Dalby, Joséa Luis Gómeza Ribelles, Gloria Gallego-Ferrer, ACS Appl. Polym. Mater. (2024)).

[14] Yifan Wu, Junwu Zou, Kai Tang, Ying Xia, Xixi Wang, Lili Song, Jinhai Wang, Kai Wang, Zhihong Wang, Burn. Trauma 12 (2024)) tkae013.

[15] Vlad Jarkov, Scotta James Allan, Chris Bowen, Hamideh Khanbareh, Int. Mater. Rev. 67 (2022)) 683–733.

[16] Nowsheen Goonoo, Fanny Gimié, Imade Ait-Arsa, Colette Cordonin, Jessica Andries, Dhanjay Jhurry, Archana Bhaw-Luximon, Biomater. Sci. 9 (2021)) 5259–5274.

[17] Chengyun Ning, Zhengnan Zhou, Guoxin Tan, Ye Zhu, Chuanbin Mao, Prog. Polym. Sci. 81 (2018)) 144–162.

[18] S. Ribeiro, A.C. Gomes, I. Etxebarria, S. Lanceros-Méndez, C. Ribeiro, Mater. Sci. Eng.: C 92 (2018)) 868–874.

[19] Xianfeng Liang, Huaihao Chen, Niana X. Sun, APL Mater. 9 (2021)).

[20] Xianfeng Liang, Alexei Matyushov, Patrick Hayes, Viktor Schell, Cunzheng Dong, Huaihao Chen, Yifan He, Alexandria Will-Cole, Eckhard Quandt, Pedro Martins, IEEE Trans. Magn. 57 (2021)) 1–57.

[21] S. Kopyl, R. Surmenev, M. Surmeneva, A. Fetisov, Mater. Today Bio 12 (2021)) 100149.

[22] Anna Rose Abraham, Balakrishnan Raneesh, Tesfakiros Woldu, Sonja Aškrabić, SašCa Lazović, Dohčević-Mitrović Zorana, Oluwafemi Oluwatobia Samuel, Sabu Thomas, Nandakumar Kalarikkal, J. Phys. Chem. C 121 (2017)) 4352–4362.

[23] Hyunseok Song, Michaela Abraham Listyawan, Jungho Ryu, Actuators 11 (2022) 380.

[24] Junsok Choi, Kia Tae Nam, Eun-Ho Sohn, Yongsok Seo, ACS Nano (2024).

[25] Kun Yue, Rakesh Guduru, Jeongmin Hong, Ping Liang, Madhavan Nair, Sakhrat Khizroev, Magneto-electric nano-particles for non-invasive brain stimulation, 2012).

[26] Kristena L. Kozielski, Ali Jahanshahi, Huntera B. Gilbert, Yan Yu, Ö. Erin, David Francisco, Faisal Alosaimi, Yasin Temel, Metin Sitti, Sci. Adv. 7 (2021)) eabc4189.

[27] Gabriele Barrera, Paolo Allia, Paola Tiberto, Emergent Mater. (2024)) 1–23.

[28] Fajer Mushtaq, Xiangzhong Chen, Harun Torlakcik, Christian Steuer, Marcus Hoop, Erdema Can Siringil, Xavia Marti, Gregory Limburg, Patrick Stipp, Bradleya J. Nelson, Adv. Mater. 31 (2019)) 1901378.

[29] Sharifia Dehsari Hamed, Kumar Manasvi, Saad Amr, Hassanpoura Amiri Moretza, Yan Chengcheng, Anwar Saleem, Gunnar Glasser, Kamal Asadi, ACS Appl. Nano Mater. 1 (2018)) 6247–6257.

[30] Wenwen Liu, Han Zhao, Chenguang Zhang, Shiqi Xu, Fengyi Zhang, Ling Wei, Fangyu Zhu, Yinga Chen, Yumin Chen, Ying Huang, Nat. Commun. 14 (2023) 4091.

[31] Margaridaa M. Fernandes, Pedro Martins, Danielaa M. Correia, Estelaa O. Carvalho, Franciscoa M. Gama, Manuel Vazquez, Cristina Bran, Senentxu Lanceros-Mendez, ACS Appl. Bio Mater. 4 (2021)) 559–570.

[32] Clarisse Ribeiro, J.A. Panadero, Vitor Sencadas, Senentxu Lanceros-Méndez, M.N. Tamaño, David Moratal, Salmerón-Sánchez Manuel, Ribelles JLa Gómez, Biomed. Mater. 7 (2012)) 035004.

[33] Bolin Tang, Junjun Zhuang, Liming Wang, Bo Zhang, Suya Lin, Fei Jia, Lingqing Dong, Qi Wang, Kui Cheng, Wenjian Weng, ACS Appl. Mater. Interfaces 10 (2018)) 7841–7851.

[34] Tanvi Jariwala, Gerardo Ico, Youyi Tai, Honghyun Park, Nosanga V. Myung, Jin Nam, ACS Appl. Bio Mater. 4 (2021)) 3706–3715.

[35] Marka I. Johnson, Carolea A. Paley, Traceya E. Howe, Kathleena A. Sluka, Cochrane Database Syst. Rev. (2015)).

[36] Melissa Marquez-Chin, Zia Saadatnia, Yu-Chen Sun, Hania E. Naguib, Milosa R. Popovic, BioMedical Eng. OnLine 23 (2024)) 10.

[37] Sujoya Kumar Ghosh, Krittish Roy, Haria Krishna Mishra, Manasa Ranjan Sahoo, Biswajit Mahanty, Prakasha Nath Vishwakarma, Dipankar Mandal, ACS Sustain. Chem. Eng. 8 (2019)) 864–873.

[38] Muhterem Koç, E.D. Dönmez, Levent Paralı, Ali Sarı, Selçuk Aktürk, J. Mater. Sci., Mater. Electron. 33 (2022)) 8048–8064.

[39] Cea Wen Nan, Ming Li, Jina H. Huang, Phys. Rev. B 63 (2001)) 144415.

[40] Ce-Wen Nan, Shuxiang Bichurin, D. Viehland, G. Srinivasan, J. Appl. Phys. 103 (2008)).

[41] Xuhao Chen, Juanjuan Zhang, Yuanwen Gao, Georgea J. Weng, Int. J. Mech. Sci. 262 (2024)) 108746.

[42] Olega V. Stolbov, Yuriya L. Raikher, Nanomaterials 14 (2023)) 31.

[43] Olega V. Stolbov, Yuriya L. Raikher, Nanomaterials 15 (2025)) 487.

[44] Paolo Allia, Gabriele Barrera, Paola Tiberto, J. Magn. Magn. Mater. 496 (2020)) 165927.

[45] Alexander Omelyanchik, Valentina Antipova, Christina Gritsenko, Valeria Kolesnikova, Dmitry Murzin, Yilin Han, Andreia V. Turutin, Ilyaa V. Kubasov, Alexandera M. Kislyuk, Tatianaa S. Ilina, Nanomaterials 11 (2021)) 1154.

[46] Bernarda Dennis Cullity, Chada D. Graham, John Wiley & Sons , Introduction To Magnetic Materials, New Jersey, 2011).

[47] Daniela B. Reeves, Johna B. Weaver, Crit. Reviews™Biomed. Eng. 42 (2014) Begel House Inc., 1.

[48] Paolo Allia, Gabriele Barrera, Paola Tiberto, Phys. Rev. B 98 (2018) 134423.

[49] Isadoraa Takako Smith, Elric Zhang, Yagmura Akin Yildirim, Manuela Alberteris Campos, Mostafa Abdel-Mottaleb, Burak Yildirim, Victoriaa Louise Ramezani, Scott-Vandeusen Aidan, Ping Liang, Wiley Interdiscip. Rev.: Nanomedicine Nanobiotechnol. 15 (2023) e1849.

[50] Gabriele Barrera, Paolo Allia, Paola Tiberto, Nanoscale 13 (2021) 4103–4121.

[51] Rashid Dallaev, Tatiana Pisarenko, Dinara Sobola, Farid Orudzhev, Shikhgasan Ramazanov, Tomáš Trčka, Polymers 14 (2022)) 4793.

[52] Gulnur Kalimuldina, Nursultan Turdakyn, Ingkar Abay, Alisher Medeubayev, Arailym Nurpeissova, Desmond Adair, Zhumabay Bakenov, Sensors 20 (2020)) 5214.

[53] Haihua Hu, Yezhen Han, Aiguo Song, Shanguang Chen, Chunhui Wang, Zheng Wang, Sensors 14 (2014)) 4899–4913.

[54] Soha Mohammadpourfazeli, Shabnam Arash, Afshin Ansari, Shengyuan Yang, Kaushik Mallick, Roohollah Bagherzadeh, RSC Adv. 13 (2023)) 370–387.

[55] Jungho Ryu, Shashank Priya, Kenji Uchino, Hyoun-Ee Kim, J. Electroceramics 8 (2002) 107–119.

[56] J. Van den, RAJ Born, J. Mater. Sci. 13 (1978) 1538–1548.

[57] Rashed Adnana Islam, Shashank Priya, Adv. Condens. Matter Phys. 2012 (2012)) 320612.

[58] M.I. Bichurin, V.M. Petrov, G. Srinivasan, Phys. Rev. B 68 (2003)) 054402.

[59] A. Kulkarni, K. Meurisch, I. Teliban, R. Jahns, T. Strunskus, A. Piorra, R. Knöchel, F. Faupel, Appl. Phys. Lett. 104 (2014)).

[60] Y.K. Vopson, Gabriel Caruntu, Gopalan Srinivasan, Materials 10 (2017)) 963.

[61] Amanda Singer, Shayok Dutta, Eric Lewis, Ziying Chen, Joshuaa C. Chen, Nishant Verma, Benjamin Avants, Ariela K. Feldman, John O'Malley, Michael Beierlein, Neuron 107 (2020)) 631–643.

[62] Dorosa N. Theodorou, Ulricha W. Suter, Macromolecules 19 (1986)) 139–154.

[63] Ting Wu, Hao Jin, Shurong Dong, Weipeng Xuan, Hongsheng Xu, Leihe Lu, Zijing Fang, Shuyi Huang, Xiang Tao, Lin Shi, Sensors 20 (2020)) 1346.

[64] Grössinger Duong, Schoenhart Roland, D. Markus, J. Magn. Magn. Mater. 316 (2007) 390–393.

[65] P. Martins, R. Gonçalves, A.C. Lopes, Ea Venkata Ramana, S.K. Mendiratta, S. Lanceros-Mendez, J. Magn. Magn. Mater. 396 (2015)) 237–241.

[66] Xuejian Mu, Hao Zhang, Chenyan Zhang, Shuya Yang, J. Xu, Yicong Huang, Jie Xu, Yongcheng Zhang, Qiang Li, Xia Wang, J. Mater. Sci. 56 (2021) 9728–9740.

[67] Jia-Wei Zhang, Xuan Meng, Geng Fu, Tao Han, Fan Xu, Chatchai Putson, Xiaoxu Liu, ACS Appl. Electron. Mater. 5 (2023)) 1844–1852.

[68] Sonali Pradhan, Pratik Deshmukh, Azama Ali Khan, Anju Ahlawat, S.K. Rai, S. Satapathy, Smart Mater. Struct. 30 (2021)) 075034.

[69] Sarit Chakraborty, S.K. Mandal, B. Saha, Ceram. Int. 45 (2019)) 14851–14858.

[70] Rabah Belouadah, Laurence Seveyrat, Daniel Guyomar, Benoit Guiffard, Fouad Belhora, Sensors Actuators A: Phys. 247 (2016)) 298–306.

[71] Hassanpoura Amiri, Sharifia Dehsari Hamed Morteza, Kamal Asadi, J. Appl. Phys. 132 (2022)).

[72] Silvio Dutz, Rudolf Hergt, Int. J. Hyperth. 29 (2013)) 790–800.

[73] Arka Chaudhuri, Kalyan Mandal, J. Magn. Magn. Mater. 377 (2015)) 441–445.

[74] Tahania M. Alfareed, Yassine Slimani, Muniraha A. Almessiere, Sagara E. Shirsath, M. Hassan, Khan Nawaz, Firdosa A., Ebtesama A. Al-Suhaimi, Abdulhadi Baykal, Ceram. Int. 48 (2022) 14640–14651.

[75] Boris Gusarov, Elena Gusarova, Bernard Viala, Leticia Gimeno, Orphée Cugat, J. Appl. Polym. Sci. 133 (2016)).

[76] F. Mokhtari, M. Shamshirsaz, M. Latifi, S. Asadi, J. Text. Inst. 108 (2017)) 906–914.

[77] Pedro Martins, Xavier Moya, C. Caparrós, J. Fernandez, N.D. Mathur, Senentxu Lanceros-Mendez, J. Nanoparticle Res. 15 (2013)) 1–6.

[78] P. Martins, R. Gonçalves, S. Lanceros-Mendez, A. Lasheras, J. Gutiérrez, J.M. Barandiarán, Appl. Surf. Sci. 313 (2014)) 215–219.

[79] C. Behera, R.N.P. Choudhary, Piyusha R. Das, J. Polym. Res. 24 (2017)) 1–13.

[80] Harsha Chouhan, Maheswar Panda, Samanway Mohanta, Dinesha Kumar Shukla, J. Mater. Sci., Mater. Electron. 36 (2025)) 655.

[81] Kirill Sobolev, Valeria Kolesnikova, Alexander Omelyanchik, Yulia Alekhina, Valentina Antipova, Liudmila Makarova, Davide Peddis, Yuriya L. Raikher, Katerina Levada, Abdulkarim Amirov, et al., Polymers 14 (2022)) 4807.

[82] Abhishek Sasmal, Shrabanee Sen, Ja Arout Chelvane, A. Arockiarajan, Polymer 281 (2023)) 126141.

[83] Rubina Ghosh, Alok Barik, Manasa Ranjan Sahoo, Subhankar Mishra, Sweta Tiwary, Praveena Kumar Panda, Dalip Saini, Dillipa Kumar Pradhan, Prakasha Nath Vishwakarma, ACS Appl. Nano Materials 6 (2023) 6841–6848.

[84] Sobia K. Chacko, Raneesh Balakrishnan, Nandakumar Kalarikkal, Nebua George Thomas, ACS Appl. Polym. Mater. 6 (2024)) 1429–1438.

[85] Jordia S. Andreu, Juan Camacho, Jordi Faraudo, Soft Matter 7 (2011)) 2336–2339.

[86] Jordi Faraudo, Jordia S. Andreu, Juan Camacho, Soft Matter 9 (2013)) 6654–6664.